HIPPOCAMPUS 25:1489–1500 (2015)

Grid Cells in 3-D: Reconciling Data and Models

Timothy K. Horiuchi[1]* and Cynthia F. Moss[2]

ABSTRACT: It is well documented that place cells and grid cells in echolocating bats show properties similar to those described in rodents, and yet, continuous theta-frequency oscillations, proposed to play a central role in grid/place cell formation, are not present in bat recordings. These comparative neurophysiological data have raised many questions about the role of theta-frequency oscillations in spatial memory and navigation. Additionally, spatial navigation in three-dimensions poses new challenges for the representation of space in neural models. Inspired by the literature on space representation in the echolocating bat, we have developed a nonoscillatory model of 3-D grid cell creation that shares many of the features of existing oscillatory-interference models. We discuss the model in the context of current knowledge of 3-D space representation and highlight directions for future research. © 2015 Wiley Periodicals, Inc.

KEY WORDS: bat; hippocampus; grid cells; place cells; space representation

INTRODUCTION

Over the past 50 years, using a wide variety of research methods, scientists have made important advances toward understanding the neurobiological foundation of spatial cognition **in 2-D space**. In particular, growing experimental evidence points to the important role of the entorhinal cortex, hippocampus, and related limbic structures in the neural representation of space. First identified in rodents is a class of neurons known as **place cells**, which fire maximally when an animal occupies specific locations in a given environment, referred to as **place fields**. Place-dependent activity can change with cues from the environment (O'Keefe, 1976), is referenced to landmarks (Burgess and O'Keefe, 1996; Siegel et al., 2008), and can be modulated by context (Anderson and Jeffery, 2003; Hayman et al., 2003). Once hippocampal place fields are established in illuminated conditions, their spatial tuning persists in the dark, suggesting their role in spatial memory (see reviews in Muller, 1996; Redish, 1999; Jeffery, 2003; Anderson et al., 2006; Mizumori, 2008). Another class of cells, **grid cells**, are found in the medial entorhinal cortex (MEC) and neighboring limbic structures. Grid cells have periodic place fields that are regularly spaced on a triangular grid (Fyhn et al, 2004; Hafting et al., 2005; Sargolini et al., 2006; Hasselmo et al., 2007). MEC grid cells project to hippocampal place cells and are hypothesized to play a role in path integration and odometry (Hafting et al., 2005; Barry et al., 2007). The grid spacing of these cells increases from the dorsomedial to ventrolateral regions of the MEC (Hafting et al. 2005). **Head direction cells**, found in several limbic structures, are not sensitive to the region of space an animal occupies, but instead to the direction it is heading in a world coordinate frame (Taube et al., 1990a,1990b, Cho and Sharp, 2001; Mizumori, 2008). Peak firing of head direction cells is correlated with an animal's future directional heading by about 25–75 ms, depending on the brain region (Taube and Muller, 1998; Blair and Sharp, 1995; Stackman and Taube, 1998). Head direction neurons are believed to play a critical role in maintaining an internal estimate of orientation, resulting from angular self-motion, and for updating the space representation to account for translational self-motion (Wiener and Taube, 2005). Intracranial recordings in humans performing a virtual navigation task have revealed place cells (as described above) and **spatial-view cells**, which are active when subjects direct their gaze at a particular location in the environment; the incidence of place and spatial view cells differs in various regions of the medial temporal lobe, but they are both present in the hippocampus proper (Ekström et al.,). Similarly, studies of single-unit activity in the hippocampus of freely moving monkeys have reported both place cells (Ono et al., 1993; Nishijo et al., 1997; Matsumura et al., 1999; Ludvig et al., 2004) and spatial-view cells (Robertson et al., 1998; Georges-François et al., 1999; Rolls, 2002).

In rodents, the activity patterns of grid cells and place cells have been tied to the phase of a theta rhythm, [local field potentials (LFP) in the range of 5–12 Hz], which is prominent in the hippocampus when the animal explores an environment by locomotion and during REM sleep (Green and Arduini, 1954, 1964; O'Keefe and Recce, 1993; Louie and Wilson, 2001, Buzsáki, 2005; Hasselmo, 2005; Berg et al., 2006; Ledberg and Rodde, 2011). Numerous hypotheses have been put forward to consider the contribution of theta rhythm to space representation.

[1] **Department of Electrical and Computer Engineering, University of Maryland, College Park, Maryland;** [2] **Department of Psychology, Institute for Systems Research, University of Maryland, College Park, Maryland**

Cynthia F. Moss is currently at the Department of Psychological and Brain Sciences, Johns Hopkins University, 3400 N. Charles Street, Baltimore, MD 21218.

Grant sponsor: ONR; Grant number: N000141210339.

*Correspondence to: Timothy K. Horiuchi, Department of Electrical and Computer Engineering, University of Maryland, College Park, MD.
E-mail: timmer@umd.edu

Accepted for publication 17 April 2015.
DOI 10.1002/hipo.22469
Published online 25 April 2015 in Wiley Online Library (wileyonlinelibrary.com).

One hypothesis, for example, proposes the interference of different oscillators in the theta band (including intrinsic cell membrane oscillations) in the creation of the triangular grid field pattern (Burgess et al., 2007; Hasselmo et al., 2007; Moser et al., 2008).

Research on space representation in bats has raised many questions about the role of theta-frequency oscillations in spatial memory and navigation. Bats are mammals that have evolved a well-developed orientation and navigation system that operates **in 3-D space.** (Ulanovsky and Moss, 2008; Tsoar et al., 2011, Yartsev et al., 2011; Yartsev and Ulanovsky, 2013). Echolocating bats produce short ultrasonic signals (vocalizations or tongue clicks) and use the information in returning echoes to build 3-D spatial representations of the environment (Moss and Surlykke, in press). These animals are known to rely on binaural comparisons of echo arrival time, amplitude, and spectrum to localize the direction of objects and use the time delays between sonar signal emissions and echoes to determine the range to objects (Moss and Schnitzler, 1995).

Distance to obstacles and targets must be accurately measured for successful orientation and prey capture, and echolocating bats show specializations for accurate echo arrival time estimation to support fine resolution target ranging (Simmons et al., 1990). Because echolocation provides an interrupted flow of spatial acoustic information and because the echolocation call times and beam directions can be directly measured, the bat is a powerful animal model in which to study task-dependent sensing, attentional modulation of space perception, and memory.

Echolocating bats operate on small, intermediate and large spatial scales, which change with the behavioral goal. At small scales (i.e., short range), bats can localize sonar objects with high precision and, under some task conditions, show sub-millisecond echo arrival-time discrimination (for review, see Moss and Schnitzler, 1995). The bat engages in medium scale navigation when it forages in the presence of obstacles, such as vegetation, when it needs to localize and react differentially to targets and obstacles. At the largest spatial and temporal scales, bats will often navigate several kilometers to their nightly hunting grounds and in the case of migrating bats, hundreds to thousands of kilometers (Tsoar et al., 2011; McGuire et al., 2012).

While sensory information generally is processed in egocentric coordinates (e.g., visual information in retinotopic coordinates, auditory localization in head-based coordinates, or touch sensors in the body coordinate frame), a cognitive map that stores the relative locations and attributes of important places in the environment is necessarily represented in world-coordinates. This map is believed to be supported by an odometry system (i.e., HD cells, grid cells, and place cells) that maintains an estimate of position in the world and merges rich contextual associations acquired from the senses (landmarks, objects, etc.) to create a robust internal representation of the environment that is capable of supporting memory-based behavior (e.g., goal-based path planning).

The importance of spatial memory to the bat's natural behaviors prompted a series of investigations into the neurobiological foundations of space representation in this animal. The first neural recordings from bat hippocampus revealed place cell activity comparable to that reported in the rodent. Ulanovsky and Moss (2007) recorded from CA1 of the tethered, crawling big brown bat, *Eptesicus fuscus*, under light (echolocation and vision) and dark (echolocation alone) conditions. As bats performed a tethered mealworm chasing task in an arena, place field activity was characterized. Bat hippocampal place fields remained unchanged across sensory conditions, but interestingly, place field tuning was tightest in the time period immediately following echolocation call production, and broadened at around 400–500 ms after calls (Ulanovsky and Moss, 2011). Furthermore, bat hippocampal cells exhibited head direction tuning (Rubin et al., 2014).

In hippocampal recordings of the big brown bat, the continuous theta typically recorded from rodent was not present; instead, theta occurred in bursts, most prominently when the bat was stationary and producing echolocation calls at a high rate (see Fig. 1, Ulanovsky and Moss, 2007). The absence of continuous theta raised questions about models of hippocampal space representation. A methodological issue, however, left this question unresolved for several years. Specifically, rodent hippocampal recordings have involved studies of the animals engaged in a natural navigation mode, namely crawling; however, the bat recordings did not engage animals in their natural navigation mode, namely flight. This issue was addressed in more recent hippocampal recordings from a different bat species, the Egyptian fruit bat (see Yartsev and Ulanovsky, 2013).

Studies of Egyptian fruit bats have substantiated and extended the findings from the big brown bat. Yartsev et al. (2011) recorded from hippocampal CA1 neurons of the crawling Egyptian fruit bat and found place cells with similar place field size and firing patterns as reported in both rat and the big brown bat (Wilson and McNaughton, 1993; Ulanovsky and Moss, 2007, 2011). Hippocampal place fields in the Egyptian fruit bat were distributed throughout the test environment, and yet, as in the big brown bat, theta oscillations were recorded only in bouts (see Fig. 1). Using wireless technology that permitted hippocampal recordings in the free-flying bat, Yartsev and Ulanovsky (2013) demonstrated 3-D hippocampal place cells that fired in restricted regions of volumetric space. Moreover, 3-D place field activity emerged in the absence of continuous theta, providing compelling evidence that these oscillations are not necessary for the creation of the basic properties of hippocampal space representation in this animal.

Yartsev et al. (2011) recorded from the medial entorhinal cortex (MEC) of the crawling Egyptian fruit bat and characterized (2-D) grid cells with a triangular firing field grid pattern, as reported in rats. Oscillatory-interference models of space representation rely on theta oscillations to generate grid cell firing patterns, and yet the authors of this study found no evidence for continuous theta in MEC recordings of the Egyptian fruit bat. Here again, the data from this species require alternatives to the oscillatory-interference models to account for grid cell formation.

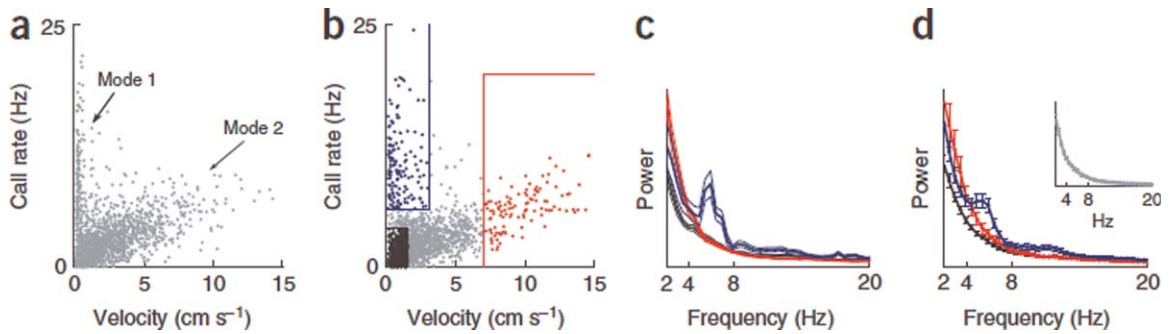

FIGURE 1. From Ulanovsky and Moss (2007). Behavior-dependent theta oscillation in the hippocampus of the big brown bat, *E. fuscus*. (a) Rate of echolocation calls versus locomotion velocity, computed in 2-s windows with 1-2 overlap (dots), showing exploratory modes 1 and 2. Data come from one recording day, pooled over sleep and waking sessions. In mode 2, the call rate was positively correlated with velocity (median correlation over all recording days, excluding mode 1 data, $r = 0.668$). For display purposes, dots were jittered in the y-direction, to compensate for the call rate discretization due to counting in a finite window (jitter size, 0.5 Hz = 1 divided by the 2 s window size). (b) Example from another recording day, with colors denoting mode 1 (blue dots), the high velocity portion of mode 2 (red dots) and low velocity call rate (black dots). The borders used for defining these three "behavioral areas" (colored lines) were the same for all recording days: velocity ≤ 3 cm s^{-1}, call rate ≥ 6 Hz (blue0; velocity ≥ 7 cm s^{-1}, call rate ≤ 20 Hz (red) velocity ≤ 1.5 cm s^{-1}, call rate ≤ 4 Hz (black). (c) Spectral power of LFP (linear scale) from one recording day, computed separately for each "behavioral area" in b (colors as in b). Thin lines are mean ± s.e.m. (d) Population average spectral power of LFP, computed by averaging single-day power spectra over all recording days from both bats; error bars are ± s.e.m. ($n = 27$ d). Main plot, behavioral sessions (colors as in b). Inset, sleep sessions. [Color figure can be viewed in the online issue, which is available at wileyonlinelibrary.com.]

To investigate the cellular physiology of principal neurons in layer II of MEC in the echolocating bat and directly test for potential theta oscillation generating mechanisms in the MEC of a species that shows hippocampal place cells, Heys et al. (2013) carried out in vitro whole cell patch recordings from neurons in layer II of MEC in slices from the adult big brown bat and compared these to recordings made in layer II of MEC in slices from the rat (postnatal 17–25 days). Data demonstrate that the membrane potential resonance frequency in MEC of the big brown bat is below 2 Hz, as compared with the theta band resonance in the rat about 8 Hz. Moreover, bat MEC neurons show overall lower resonance strength than rat. The whole cell patch data suggest that significant differences exist in the characteristic physiology of layer II principal neurons in MEC across the two species and call for alternatives to oscillatory-interference models of space coding.

While the lack of continuous theta oscillation in the bat hippocampus is not compatible with the oscillatory-interference model of grid cell creation, another major class of models for grid pattern creation, the 2-D attractor models (e.g., McNaughton et al., 2006; Burak and Fiete, 2009; Guanella et al., 2007), also have limitations. In 2-D attractor models, the grid pattern is defined by recurrent, inhibitory-surround synaptic connectivity. These models have the primary advantage of accounting for the existence of the 2-D triangular grid fields of MEC neurons without theta oscillations and at all spatial phases; however, they also require extensive and highly specific synaptic connectivity to move these patterns of activity across the grid cell layers in response to animal movements. Furthermore, to extend this type of model to 3-D, spherically recurrent, surround wiring, and the infrastructure to support the 3-D translation of neural activity becomes an enormous challenge. Inhomogeneities in the neural and synaptic properties can produce local minima in the activity pattern, which make translation problematic unless it is directly addressed (Burak and Fiete, 2009). To understand the bat hippocampus and the underlying mechanisms of 3-D grid cells, a new form of model is needed to reconcile comparative data on space representation. Here, we present a new grid cell model that extends very naturally into higher dimensions.

METHODS AND RESULTS

A Theta-Free Model of 3-D Grid Cell Creation

We propose a model for the 3-D bat grid cell that offers the simplicity and advantages of oscillatory-interference models, but does not use oscillatory phase to represent position. Extending a simplified version of the 2-D grid cell model of Mhatre et al., 2012 (see also Grossberg and Pilly, 2012) that uses three ring-integrator networks for encoding two spatial dimensions (i.e., "stripe cells"), we add a fourth ring-integrator network and adjust the orientations of the tuning vectors appropriately for 3-D.

In this model, the ring-integrator is a ring of neurons configured as a 1-D attractor network that has local, recurrent, synaptic connections (excitatory center with an inhibitory surround) and a global feedback inhibitory neuron to ensure that neural activity consistently occurs at only one location on the ring (see Fig. 2). The network additionally contains neurons and

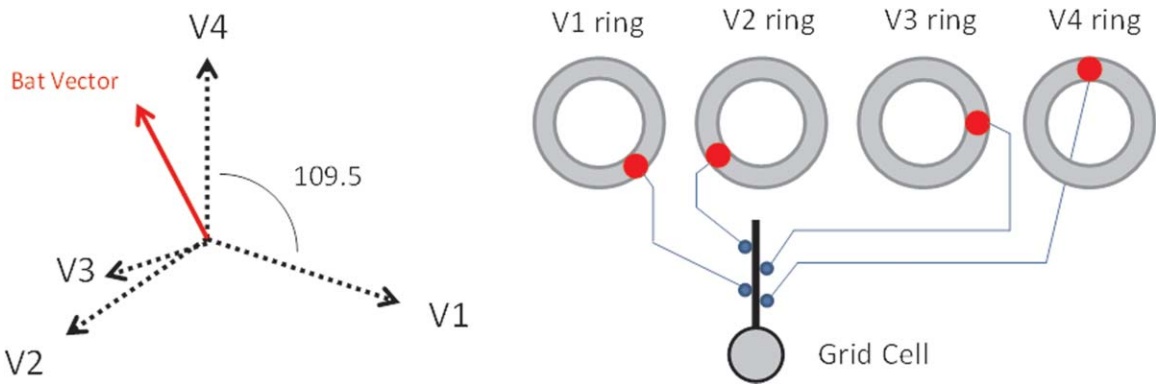

FIGURE 2. 3-D Grid Cell Model. Left: A three-dimensional movement vector (thick red arrow) is projected onto each of the four ring-integrator orientations. The resulting vectors are then translated into a rotational phase rate that moves the bumps around each ring. Projection vectors with "+"signs produce positive phase rotations and vectors with "−"signs produce negative phase rotations. Note that these vectors are defined in the world frame of reference (allocentric). Right: A small group of neurons from each ring representing a particular phase project their activity to a single grid cell configured to detect a four-way coincidence using saturating synapses to simulate a multiplication. [Color figure can be viewed in the online issue, which is available at wileyonlinelibrary.com.]

connections that give the network the ability to move the "bump" of neural activity around the ring in response to translational movements of the animal. When there is no translational motion, the bump of activity on the ring does not move around the ring. Each ring-integrator is associated with a particular allocentric 3-D reference vector in space (e.g., V1 in Fig. 2) and its activity bump rotates around the ring with a rate proportional to the projection (i.e., inner-product) of the animal's 3-D translation ("Bat Vector" or BV) onto the ring-specific vector. Specifically, $\dot{\theta}_i = \alpha(V_B \cdot V_i)$, where θ_i is the phase of the i-th ring-integrator, V_B is the bat's 3-D movement vector, and V_i is the ring-specific "reference" vector. Note that the rotation can occur in either direction around the ring. These ring-integrators integrate velocity signals to hold a periodic estimate of the animal's position along the reference vector's direction. For a 3-D grid cell, the four ring-integrators have reference vectors uniformly separated by 109.5°. The individual neurons of the ring-integrator circuit correspond to the "stripe" or "band" cells described in the parasubicular and medial entorhinal cortex (Sargolini et al., 2006; Krupic et al., 2012), showing firing fields that appear as stripes in the 2-D environment. The 3-D "stripe cells" would define oriented planes in 3-D space that intersect at lattice points (a 2-D example of intersecting stripe patterns is shown in the middle panel of Fig. 3) that correspond to a face-centered cubic lattice, which has been described as an optimal tiling for encoding positions in space efficiently (Mathis et al., 2013). Interestingly, the specifications of this proposed ring-integrator network are identical to models of the head-direction cell system (e.g., McNaughton et al., 2006) except that it is driven by translational movement inputs instead of angular velocity. The discretization of the ring location (due to finite number of elements), recurrent excitation, and winner-take-all functionality of the ring-integrator create weak local minima that can resist drifting of the activity bump around the ring due to noise (or intended movements).

In this model, each 3-D grid cell receives synaptic inputs from a single location on each of the four ring-integrators. The grid cell is active only if all four inputs are active. This logical AND operation causes the cell to fire only at the four-way intersections of the 3-D stripe cell planes. Grid cells with inputs from different locations on the rings have different phases in their spatial firing patterns. The spatial frequency of the grid pattern depends on the mapping gain (α in the equation above) between translational movements in the world (in meters per second) to the rotation rate of the activity bumps in the ring-integrators (in radians per second). Increasing the mapping gain leads to higher spatial frequencies as the stripe cells fire more frequently for a given distance traveled. This method provides flexibility in creating multiple spatial frequencies and in modulating the spatial frequency of existing cells.

In our analytical model (with no temporal dynamics), the spatial pattern of activity in the ring-integrators is Gaussian:

$S_{n,i}(\theta_i) = A \cdot e^{\frac{-(\mathrm{mod}(\theta_i,2\pi)-\pi-\theta_{\mathrm{offset}\_n})^2}{\sigma^2}}$ where $S_{n,i}$ represents the activity of the n-th neuron on the i-th ring-integrator and the phase$\theta_i$represents the integrated velocity on the ring. In this work, $A = 1$. The modulo (mod) function creates a sawtooth function from θ_i and the Gaussian is centered at $\pi/2$ and the offset places the Gaussian at different points around the ring. Grid cells are driven by the four-way conjunction of activity from neurons on the different rings. This is implemented in the model by multiplication followed by a linear activation function: $G_j = f\left(S_{a,1}(\theta_1) \cdot S_{b,2}(\theta_2) \cdot S_{c,3}(\theta_3) \cdot S_{d,4}(\theta_4)\right)$ where a, b, c, and d are the indices for the neurons from the four rings that drive this particular grid cell. $f(x) = x$ for $x > 0$. Such a multiplication can be approximated by the biologically plausible summation of logarithmically compressed inputs and with appropriate modifications to f. While the specific shape of activity on the ring-integrators (e.g., Gaussian) and the method of detecting the four-way conjunction affect the shape of the

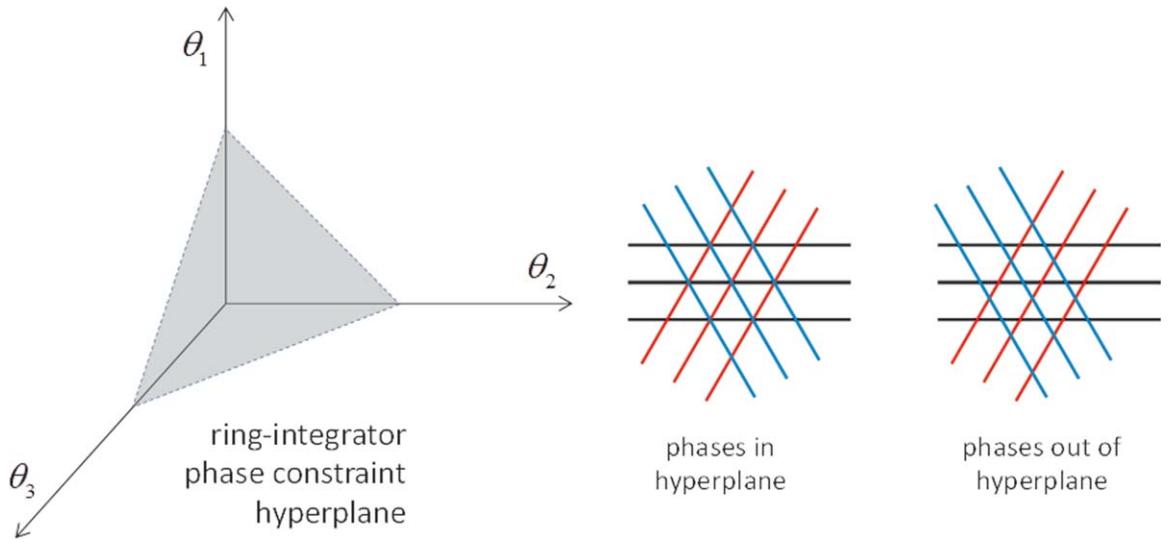

FIGURE 3. Phase space constraint for a 2-D example. A 2-D grid cell uses three ring-integrators configured for motion in three different directions: 0, 120, and 240°. The individual neurons of a given ring-integrator are stripe cells with different phases along the same direction. The 2-D grid cell fires when all three of its inputs (from different rings) are active. This occurs in the example on the left, "phases in hyperplane." This requires a specific phase relationship between the ring-integrators. For the three ring-integrators used for 2-D, the phases must stay on a plane defined by: $\theta_1 + \theta_2 + \theta_3 = C$, where C is a constant. If the phases leave the hyperplane, as in the example on the right, there will not be three-way intersections and the grid cell will not fire. [Color figure can be viewed in the online issue, which is available at wiley onlinelibrary.com.]

grid fields, they do not change the phase or frequency of the basic grid pattern. The resulting grid fields (see Fig. 4 for a 2-D example and Fig. 5 for a 3-D example) can appear more binary due to the sigmoidal activation function of the neuron. Here, in the analytical model, we do not implement recurrent, inhibitory feedback on the grid cell population (Buetfering et al., 2014) but note that this could have an important role to play in defining the neural firing thresholds and resulting spatial tuning.

One important requirement with this model (in common with oscillatory interference models) is that the phases of the four ring-integrators encoding 3-D space must maintain a specific relationship to each other to ensure that all four of the "stripe" patterns will overlap at some point. An example of the

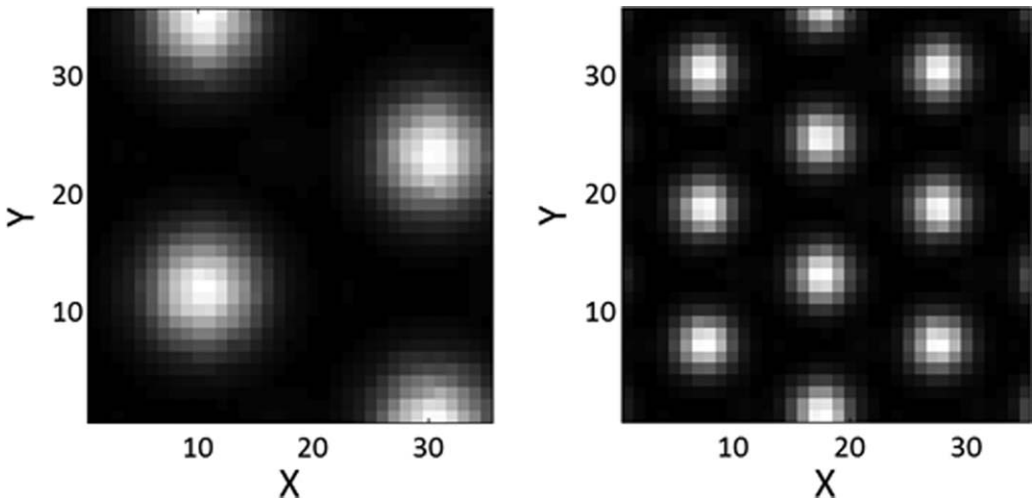

FIGURE 4. Two examples of horizontal slices through the 3-D spatial grid field produced by two grid cells of different spatial frequency. This plot was created by simulating an animal moving throughout the environment and plotting the strength of activation. Different spatial scales are produced by scaling the parameter α that determines the translation from linear movement speed in the world to ring-integrator phase rate. The left panel uses model parameters: σ = 0.565 radians and α = 0.262 radians per step and the right panel uses: σ = 0.565 radians and α = 0.524 radians per step.

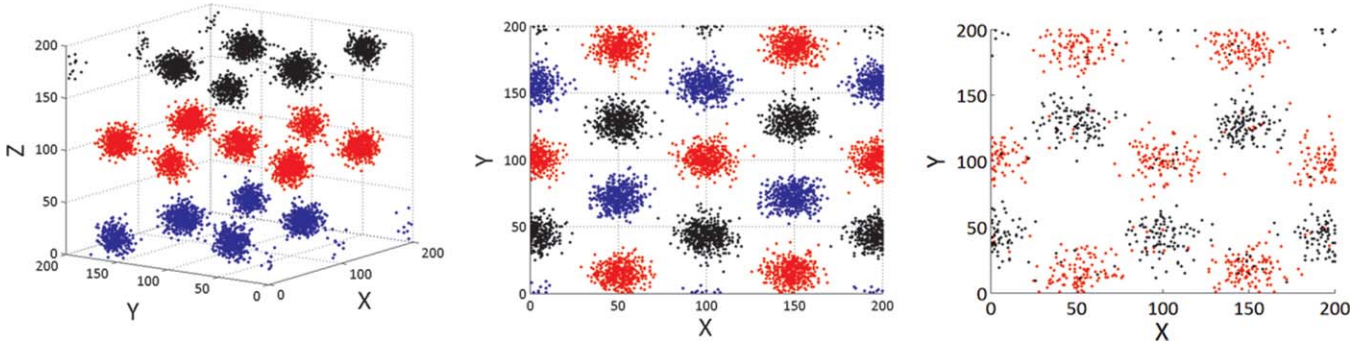

FIGURE 5. A 3-D grid firing field created by the four ring-integrator system. The amplitude of is used to Colors are used to simplify visualization of the fields at different z-axis values. Left: an angle view showing the triangular grid that occurs in each layer. Middle: a top view showing relative alignment of the triangular grids when viewed from the top. These three layers repeat vertically above and below the shown volume. This pattern is known as a face-centered cubic lattice. Note that at *z*-axis values between two layers, if the firing fields are large enough to overlap, a weak hexagonal grid pattern emerges. Right: A thin horizontal slice of the pattern at $z = 120$ to 160 to show the hexagonal grid pattern when the fields are large enough to overlap between field layers. Model parameters were: $\sigma = 0.565$ radians per step and $\alpha = 0.942$ radians. [Color figure can be viewed in the online issue, which is available at wileyonlinelibrary.com.]

importance of this phase relationship is shown in Fig. 3 for a 2-D example for ease of visualization.

In 3-D, the phases of the four ring-integrators should obey the hyperplane equation $\theta_1 + \theta_2 + \theta_3 + \theta_4 = C$, where θ_i is the phase of ring-integrator i and C is a constant that defines the offset (from the origin) of the constraint hyperplane (see Fig. 3). Once the correct phase relationship is obtained, accurate integration of 3-D movement in the ring-integrator will keep the phases on the appropriate plane. If we move off this plane, however, the chosen combination of phases of the four ring-integrators (for a given grid cell) will not recur and the grid cell will not be activated for any position. Errors encountered in the velocity encoding or integration of the velocity in the ring networks have the potential to produce a drift off of the desired phase plane. It should be noted that this phase plane issue is also important for oscillatory interference models and is not unique to our model. How this can be enforced or actively managed in the biological system is an open question, however, reciprocal excitatory connections between grid cells and the ring-integrators that support valid in-plane patterns of activity could operate as a planar attractor to correct perturbations off the correct phase plane. This issue is discussed further in the next section on dynamical models.

This model network has a number of desirable properties in the context of this scientific literature on space representation. First, the model does not use theta oscillations to create the grid pattern, consistent with the bat hippocampal data. Second, the creation of 3-D grid cells (hypothesized for use in generating 3-D place cells) is simply created by adding a fourth ring-integrator to the 2-D model by Mhatre et al. (2012) and by orienting the 3-D reference vectors 109.5° from each other. Third, updating the grid cell activity as the animal moves is performed on the four 1-D ring-integrators instead of on a higher-dimensional map. Fourth, the model uses a ring-integrator network model (1-D attractor network) that is nearly identical to those postulated for the head-direction cell system (e.g., Zhang, 1996; McNaughton et al., 2006; Massoud and Horiuchi, 2011).

One interesting consequence of these phase-based models is that the grid cells can be driven solely by the 1-D ring-integrator networks and do not rely on the activity of other grid cells, allowing the phase and spatial frequency properties of a given grid cell to be independent of neighboring grid cells. This, of course, does not preclude interactions between grid cells, nor the organization of grid cells with respect to phase or spatial frequency (Hafting et al., 2005; Brun et al., 2008; Stensola et al., 2012) that might arise due to correlated firing patterns (Bush and Burgess, 2014).

A Dynamical Model of the Ring-Integrator

While the ring-integrator and grid cell model have thus far been described in terms of feedforward analytical modules, the neurobiological implementation is likely to be a recurrent network with important dynamics. For example, the 1-D ring-integrator can be implemented with neurons that have recurrent lateral excitation and global feedback inhibition. In such a network, the interconnections couple the elements, often reducing the dimensionality of the system and limiting the range of patterns that can occur on the network (in this case, a line-attractor) and that resist perturbations away from these states. In this section, we have implemented the ring-integrator using N "neuron units" (that are simplified neural models representing average firing rates with continuous variables) that use time-domain differential equations to show how the feedforward analytical functions described above might be implemented and understand how these systems respond to perturbations. The neuron model is based on the leaky integration of different inputs at the hidden internal state, u, that is

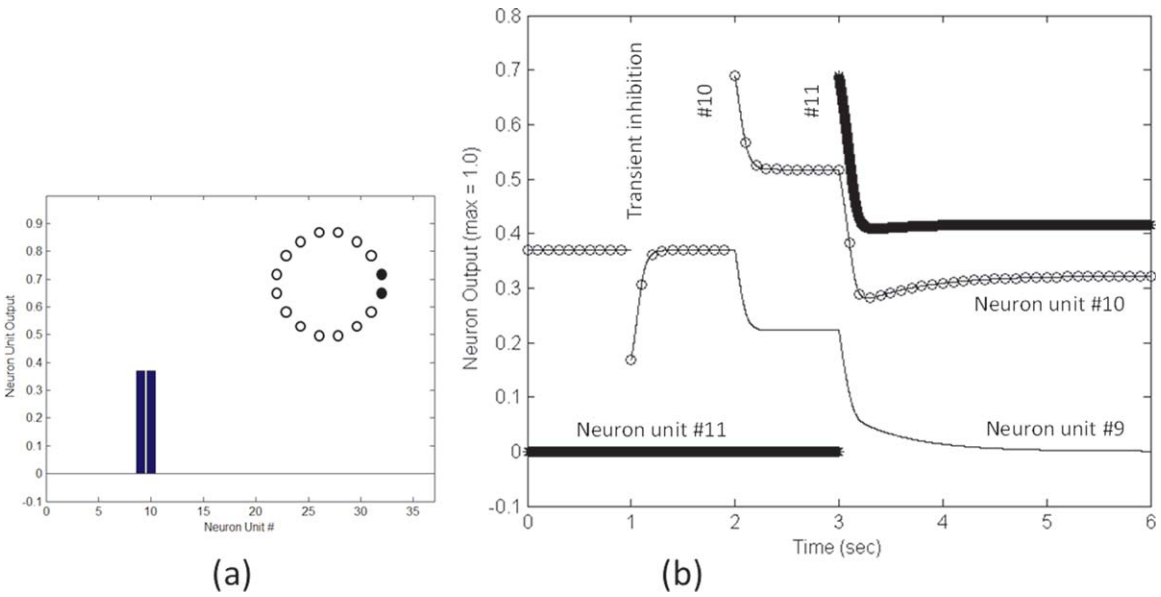

FIGURE 6. The N-element ring-integrator is designed to be a line-attractor in N-dimensional space. To demonstrate the effect of perturbations on the network, a dynamical simulation was performed. In this ring-integrator model (with 32 neuron units), the steady-state response is one where two neighboring neuron units on the ring are equally activated [See panel (a)]. For this example, the outputs of neuron units #9, #10, and #11 are shown [See panel (b)]. Initially, neuron units #9 and #10 are firing equally at ~38% of the maximum level and Neuron unit #11 is not active. At $t = 1.0$ sec, Neurons #9 and #10 are both transiently suppressed, resulting in the reduction of inhibition and a rapid recovery of both units. At $t = 2.0$ s, Neuron unit #10 alone is transiently excited, increasing the overall inhibition of the ring resulting in a rapid suppression of both units #9 and #10 until a new "equilibrium" is reached. This not a true equilibrium, as it will return to the initial condition with a long time constant (~20 s). At $t = 3.0$ s, neuron unit #11 is excited, leading to a new inhibitory surge that suppresses neuron unit #10 to a new nonzero level and suppresses unit #9 completely. The network allows the activity to move around the ring and be temporarily maintained as a memory (i.e., movement along the line attractor in N-dimensional space), but opposes perturbations that move the activity away from the N-dimensional "line attractor" (e.g., the perturbation at $t = 1.0$). [Color figure can be viewed in the online issue, which is available at wileyonlinelibrary.com.]

represented at the output by the saturating hyperbolic tangent function, $f()$.

$$\frac{du_j}{dt} = -\alpha_R \cdot u_j + \sum_{i=1}^{N} w_{ij} \cdot R_i + I_{bias} + w_{inh} \cdot RI \; j = [1, N]$$

$$R_j = f(u_j)$$

$$\frac{du_{inh}}{dt} = -\alpha_I \cdot u_{inh} + \sum_{j=1}^{N} w_{j,inh} \cdot R_j$$

$$RI = f(u_{inh})$$

$$f(x) = 0.5 + 0.5 * \tanh(8x - 4)$$

In these equations, α controls the "leakiness" of the neuron units, w_{ij} represents the sparse matrix of recurrent lateral excitation to the neighborhood of each neuron unit, w_{inh} represents the weight of feedback inhibition, and $w_{j,\text{inh}}$ represents the excitatory weight from the ring-integrator units to the global inhibitory (GI) neuron unit. In the simulations shown in Figure 6, the ring-integrator neuron units only excite their nearest-neighbor and themselves (i.e., w_{ij} is tridiagonal). This results in low spatial duty-cycle activation on the network that highlights the discrete nature of the ring-integrator. We thus approximate a line-attractor with a tightly spaced ring of point attractors. The network is initially shown in steady-state with a narrow "bump" of activity at unit locations 9 and #10. The simulation shows the differential response to perturbations that push the network state away from the "line-attractor" (e.g., $t = 1.0$) and along the "line-attractor" (e.g., $t = 2.0$ and $t = 3.0$).

Ring-Integrator Phase Constraint Network

As discussed in earlier sections, a key requirement of the ring-integrator approach is that the phases of the ring-integrators maintain a specific relationship to each other ($\sum_n \theta_n = C$) to ensure that the grid cells continue to receive coincident inputs (see Fig. 3). In this section we propose a method for maintaining this relationship in the face of noise, drift, and imperfect velocity integration (Fig. 7).

In the model, specific ring-integrator phase combinations (or "phase vector") excite the grid cells using coincident excitatory inputs to create the triangular grid pattern. By hypothesizing reciprocal excitatory projections from the grid cells back to the ring-integrator neurons, a positive feedback loop is created, supporting the specific phase-vector that best excites a given

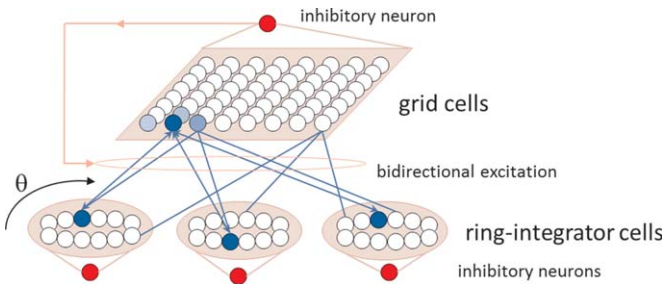

FIGURE 7. Modified network architecture for implementing a phase plane constraint (2-D example). In this simulation, three ring-integrator networks excite the grid cells such that each grid cell has a different spatial phase tuning. Reciprocal excitatory connections from the grid cells back to the ring-integrator cells create attractor states that can shift activity in both grid and ring-integrator cells to valid (on-plane) combinations. [Color figure can be viewed in the online issue, which is available at wileyonlinelibrary.com.]

grid cell. A given combination of active ring-integrator neurons and a grid cell operates as a point attractor on the desired phase plane with an attraction neighborhood defined by the spatial specificity of the grid cell. With sufficient overlap in individual grid cell properties, we create an approximation to the planar attractor with tightly spaced sheet of point attractors.

By design, when the ring-integrators are operating on the desired phase plane, a large number of grid cells will be active (e.g., Fig. 8a) and when the phase vector is not centered on the desired phase plane, only a small number of grid cells will be active (e.g., Fig. 8b).

The collective feedback from the population of active grid cells will overlap and nudge the phase vector toward the desired phase plane (but generally not towards any specific point attractor). To prevent overwhelming positive feedback when operating correctly on the plane (many active grid cells), yet allowing unambiguous corrective feedback when operating off but near the plane (few active grid cells), the feedback excitation is inhibited by the grid layer inhibitory feedback neuron (GI) that activates strongly once a moderate population of grid cells becomes active. In addition, the strong winner-take-all nature of the ring-integrator networks will prevent an ambiguous result. If the phase vector is so far off the plane that no grid cell fires sufficiently to activate the feedback excitation, the phase vector will not be corrected.

Figure 9 shows an example of the ring-integrator activity for a phase vector that is off the desired plane (Fig. 9a) and the resulting ring-integrator activity after the phase vector has been shifted back onto the plane (Fig. 9b). Figure 10 shows the temporal dynamics of the phase sum as it is brought back towards the plane from many different starting points. There is an attraction region where the phase vector is restored onto the plane and a region where the feedback does not correct the phase vector.

This mechanism also provides a means for "resetting" the ring-integrator to a particular state by strongly driving a particular grid cell. This could be important for correcting drift in the velocity integration process.

DISCUSSION

Comparative hippocampal data are important to the development, refinement and testing of models of space representation. Recordings from the bat hippocampal formation, for example, have challenged the generality of well-established

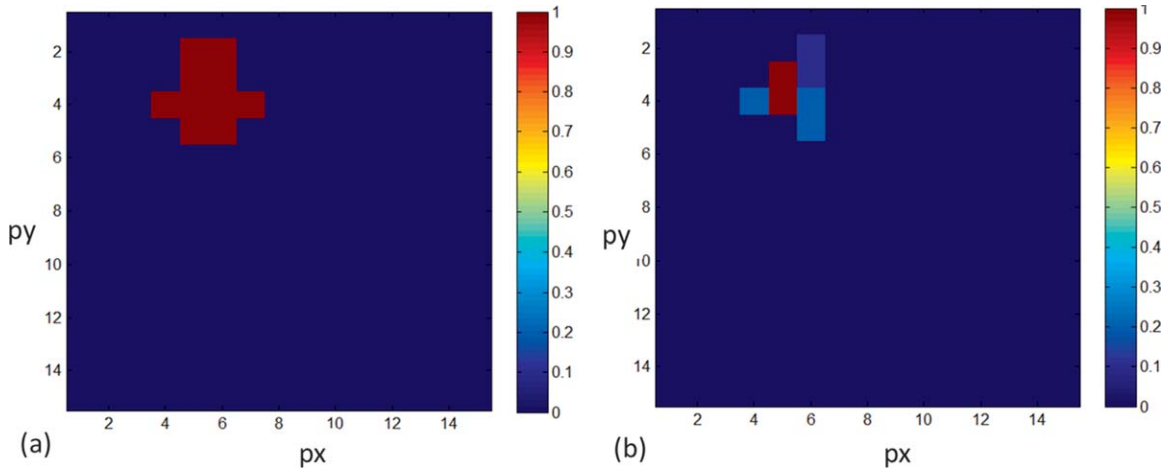

FIGURE 8. Activation of the Grid Cell Layer (2-D example). In this display, grid cells with similar 2-D grid field phase selectivity are shown next to each other. Panel (a) shows the normalized activation of a portion of the grid cell layer for a ring phase vector that lies on the desired phase plane. The phase vector is very similar to the example in Figure 9, panel (b). A group of grid cells are strongly active. Panel (b) shows an example of the normalized activation of a portion of the grid cell layer in response to a ring phase vector that is some distance from the desired phase plane ("off-plane"). Note that while only a few neurons are active, they are strongly active. This is important for providing strong corrective feedback to the ring neurons. [Color figure can be viewed in the online issue, which is available at wileyonlinelibrary.com.]

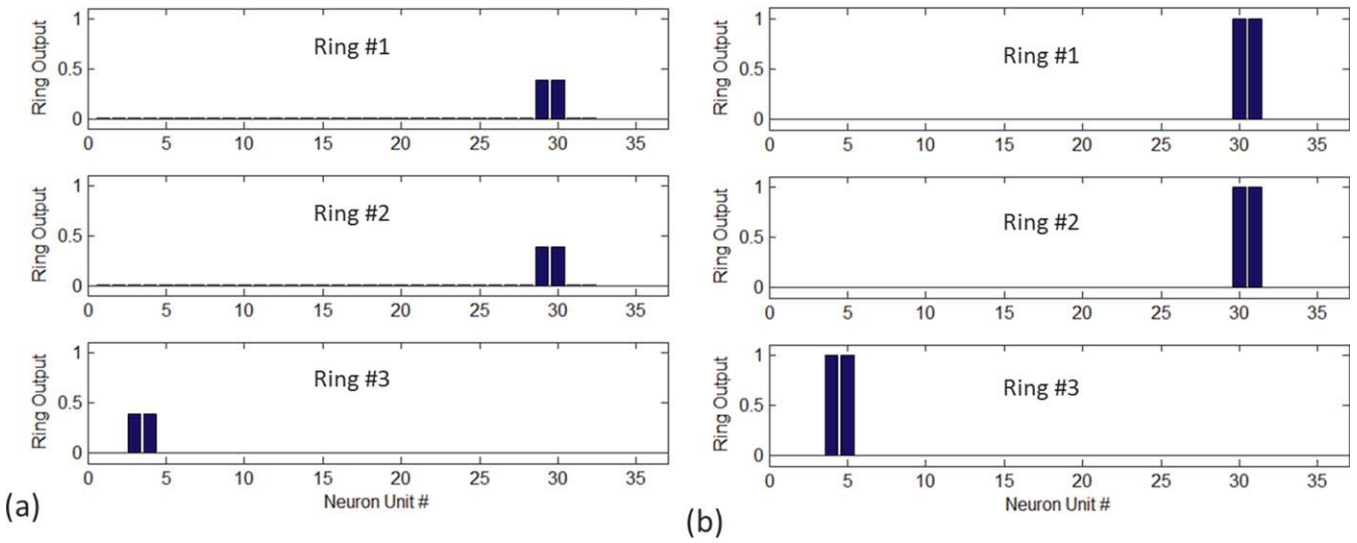

FIGURE 9. Modulated reciprocal connections between the ring-integrators and the grid cell layer nudge the ring phases to lie on the phase constraint plane. Panel (a) shows an initial off-plane state before adaptation [e.g., Fig. 8, panel (b)]. Grid cells are receiving weak excitatory drive due to the lack of coincident input; a few grid cells, however, are active. In this state, some ring neurons are receiving strong corrective excitatory feedback from the active grid cells. Panel (b) shows the steady-state condition following corrective feedback. Activity in all three rings has rotated (shifted to the right), resulting in strong drive at the grid cell layer for many cells. The increased feedback to the ring networks has boosted their activity level. This boost is limited by the now-active grid cell layer GI neuron to prevent over-stimulation due to the larger number of grid cells that are active. [Color figure can be viewed in the online issue, which is available at wileyonlinelibrary.com.]

models that rely on continuous theta. Indeed, the lack of continuous theta in bats suggests that the oscillatory interference model cannot be used to describe the bat's grid cell system, and the expansion of grid cell coding into three dimensions challenges multi-dimensional attractor models (e.g., 2-D attractor model). The model presented here offers a viable alternative. Closely related to the oscillatory-interference model, an animal's motion (projected onto different reference vectors) is integrated on multiple ring-integrators to represent position in the location of the activity (i.e., phase) on the ring. Grid field patterns are created by neurons that are selective to specific combinations of ring-integrator phases that occur periodically in space. The proposed hybrid model relies on the stability of a one-dimensional attractor network (the ring-integrators) for storing position and constructs the grid pattern through spatial interference patterns.

An interesting question that arises when considering an animal operating in 3-D is the question of how the odometry system behaves when the animal is traveling along a 2-D surface. The 3-D grid cell model can revert to a 2-D grid cell model by eliminating the dependence on the vertical dimension. By activating all of the elements in the ring-integrator that responds exclusively to vertical movement (by suppressing its global feedback inhibition) and by inhibiting (i.e., setting to zero) the motion signal from the z-axis measurement in the velocity calculation for the remaining three ring-integrators, all of the grid cells will show periodic activity in the current movement plane (Fig. 11).

A key question remains for all nonoscillatory models, "What then is the role of the theta oscillation?" Theta oscillations provide the framework in which phase-precession can be described for the rat, implying that during periods without such an oscillation, phase precession (and therefore its computational function, if any) is not occurring. Is phase precession the deliberate result of driving the place cell network to scan along a particular path? The expansion of the bat place field following vocalizations may provide a clue. If the place field expansion, as suggested above, is the result of network relaxation following a period of sensory driven responses, phase precession might be the natural evolution of activity in the hippocampal network in the intervals between the periodic drive from the odometry system at theta frequencies (i.e., grid cells). Place cells that are linked to each other could produce a brief cascade of activation resembling a path starting from this location before the next wave of activation arrives from the grid cells.

In the bat literature, there remain gaps that call for additional studies to develop a unified understanding of the allocentric representation of space across species. For example, hippocampal recordings from the crawling big brown bat, *E. fuscus*, revealed bouts of theta that occurred when the animal was relatively stationary and producing echolocation calls at a comparatively high rate (Ulanovsky and Moss, 2007). These data suggest that theta may be present in the echolocating bat when it actively attends to sonar objects. Human and monkey hippocampal studies have shown similar data, with intermittent bouts of theta separated by desynchronized periods of nontheta

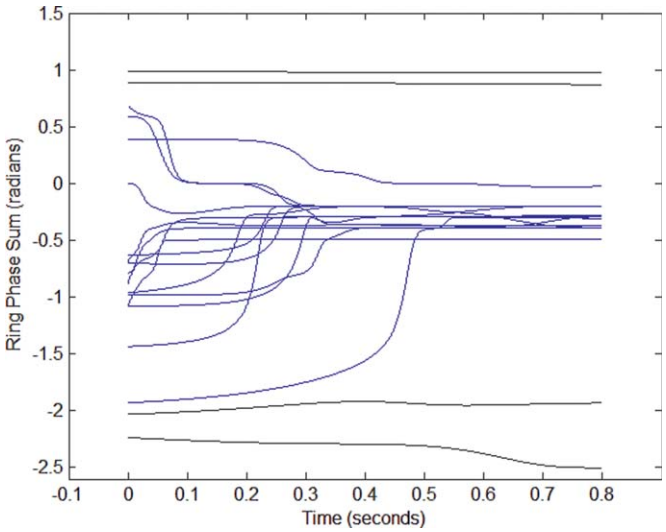

FIGURE 10. The phase constraint network brings the phase vector $\bar{\theta} = (\theta_1, \theta_2, \theta_3)$ back onto the plane defined by, $\theta_1+\theta_2+\theta_3 = C$ where the different "stripe" patterns produce 3-way intersections. In this case, $C \approx 0$. Reciprocal connections between grid cells and ring-integrator cells create attractor states that draw the phase vectors to lie on the desired plane, which results in robust grid cell activity. Each trajectory begins with the phase vector off-plane and a correction to the desired phase plane occurs if the starting phase vector is not too far away from the plane. The phase vectors representing the end states of each trace represent the firing of different grid cell groups. Discretization of the different grid cell properties (e.g., the preferred grid phase of a given grid cell) along with the suppression of feedback signals when "enough" grid cells are active, results in a range of final phase sums. [Color figure can be viewed in the online issue, which is available at wileyonlinelibrary.com.]

(Ekström et al., 2005; Jutras et al., 2013) and higher theta power associated with better task performance (recognition memory; Jutras et al., 2013). The free-flying bat shows a much larger repertoire of adaptive call behavior than a crawling bat (e.g., Moss and Surlykke, in press), and tapping into this natural behavior allows for a more complete test of the relation between sonar attention to objects and bouts of theta. Specifically, as the echolocating bat inspects sonar objects, it produces sonar strobe groups, clusters of calls with relatively stable, short intervals, flanked by calls at longer intervals (Moss et al., 2006). The bat's production of sonar strobe groups is a reliable indicator of its spatial attention to objects in the environment (Kothari et al., in press). Therefore, an important next step in this line of research is to obtain hippocampal recordings from a free-flying echolocating bat that is actively (and observably) investigating its environment by sonar. Recordings from free-flying Egyptian fruit bats, *Rousettus aegyptiacus*, for which hippocampal and MEC data have been published (Yartsev et al., 2011; Yartsev and Ulanovsky, 2013), do not yield the necessary data, as this species produces tongue clicks at relatively fixed intervals as it seeks food and avoids obstacles. Moreover, the Egyptian fruit bat is highly visual and relies primarily on sonar to navigate in dark caves. Therefore, it is critical to investigate theta power in a laryngeal echolocating bat that dynamically adjusts its sonar call rate in response to echo information collected from the environment. It may be that theta power will coincide with the bat's production of sonar strobe groups at points in time when it attends to targets and obstacles. There are, however, classes of models (such as the one presented here) that do not rely on theta oscillations in space representation.

The tuning of some hippocampal place fields measured in a crawling bat is sharpest immediately after a sonar vocalization and broadens over time. The time scale over which bat hippocampal place fields show changes in tuning is 50–500 ms, which represents a portion of the natural range of call intervals used by many lingual echolocators (Ulanovsky and Moss, 2011). It is important to note that the sonar call rates of a crawling bat are far lower than those of a free-flying bat. As the echolocating big brown bat forages, its call rate increases from 5 to 10 calls/sec to over 150 calls/s as it searches, tracks and intercepts insect prey on the wing (Surlykke and Moss, 2000). Thus, the intervals for echo processing span 6–200 ms, raising questions about bat hippocampal place field tuning as the animal dynamically modulates the rate of its calls in flight. Does the bat's production of calls at a high rate contribute to improved navigation performance and a sharpened representation of space? In other words, is place field tuning tightest when a bat produces calls at a high rate? When it directs its attention to a target? We hypothesize that there is a general relationship between sensory sampling and space representation that unifies comparative studies of place cell activity in mammals. This hypothesis applies to all animals that sample

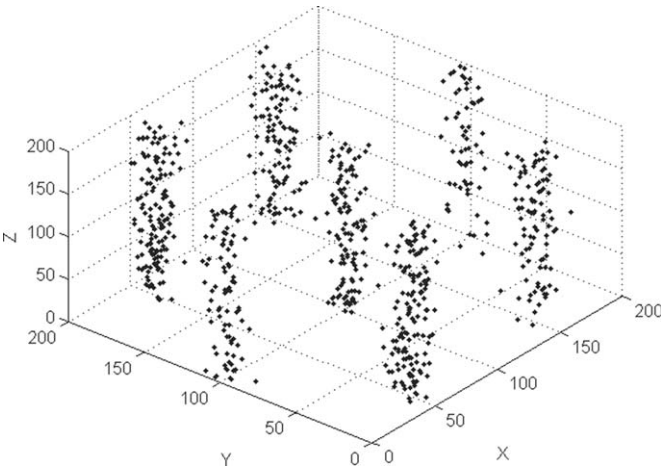

FIGURE 11. Operating the 3-D model in 2-D. By activating all elements of the ring-integrator that respond to purely vertical motion and inhibiting (i.e., set to zero) the motion signal from the z-axis measurement in the calculation of phase-rate for the remaining three ring-integrators, the 3-D model reverts to 2-D operation as seen in the rat experiments of Hayman et al., 2011. Both modifications can be implemented by inhibitory inputs to the system: (1) suppression of the global inhibition unit of the ring-integrator (i.e., disinhibition) and (2) suppression of the vertical motion signal prior to calculation of the phase rates. Model parameters were: $\sigma = 0.565$ radians and $\alpha = 0.0785$ radians per spatial unit.

information from the environment on different time scales, for example visual animals that move their eyes to foveate and attend to objects distributed across space and rodents that whisk to investigate their proximal environment. Hippocampal recordings from a free-flying laryngeal echolocator that dynamically adjusts its sonar calls in response to objects in the environment can be used to test this hypothesis.

It should be noted that if grid cell activity is used to define place cell activity, sharpening of grid cell field responses could also sharpen place cell tuning. The parvalbumin interneuron inhibitory network present in the MEC (Buetfering et al., 2014) could provide the mechanism to sharpen grid cell responses by up-regulating inhibition during sonar vocalizations, then allowing it to relax in the intervals between vocalizations, resulting in broader firing fields.

As a final note, it interesting to consider that hippocampal odometry models assume that the careful mathematical integration of velocity to estimate position is its primary function and that sensory inputs and prior experience can be used to correct for the accumulation of errors. For a flying or swimming animal, however, the accurate determination of 3-D velocity with respect to the ground is fraught with challenges and seems to predict significantly lower odometry performance compared to animals directly in contact with the ground. Echolocation, on the other hand, can directly provide the animal with its position (i.e., distance) relative to environmental objects. How is echolocation information used to drive odometry or provide corrective information? Our future modeling efforts will address this question.

ACKNOWLEDGMENTS

The authors thank Nachum Ulanovsky for helpful comments on an earlier draft of this manuscript.

REFERENCES

Anderson MI, Jeffery KJ. 2003. Heterogeneous modulation of place cell firing by changes in context. J Neurosci 23:8827–8835.

Anderson MI, Killing S, Morris C, O'Donoghue A, Onyiagha D, Stevenson R, Verriotis M, Jeffery KJ. 2006. Behavioral correlates of the distributed coding of spatial context. Hippocampus 16:730–742.

Barry C, Hayman R, Burgess N, Jeffery KJ. 2007. Experience-dependent rescaling of entorhinal grids. Nat Neurosci 10:682–684.

Berg RW, Whitmer D, Kleinfeld D. 2006. Exploratory whisking by rat is not phase locked to the hippocampal theta rhythm. J Neurosci 26:6518–6522.

Blair HT, Sharp PE. 1995. Anticipatory head direction signals in anterior thalamus: evidence for a thalamocortical circuit that integrates angular head motion to compute head direction. J Neurosci 15: 6260–6270.

Brun VH, Solstad T, Kjelstrup KB, Fyhn M, Witter MP, Moser EI, Moser MB. 2008. Progressive increase in grid scale from dorsal to ventral medial entorhinal cortex. Hippocampus 18:1200–1212.

Buetfering C, Allen K, Monyer H. 2014. Parvalbumin interneurons provide grid cell-driven recurrent inhibition in the medial entorhinal cortex. Nat Neurosci 17:710–718. doi:10.1038/nn.3696.

Burak Y, Fiete IR. 2009. Accurate path integration in continuous attractor network models of grid cells. PLoS Comput Biol vol. 5: e1000291- doi: 10.1371/journal.pcbi.1000291

Burgess N, O'Keefe J. 1996. Neuronal computations underlying the firing of place cells and their role in navigation. Hippocampus 6: 749–762.

Burgess N, Barry C, O'Keefe J. 2007. An oscillatory interference model of grid cell firing. Hippocampus 17:801–912.

Bush D, Burgess N. 2014. A hybrid oscillatory interference/continuous attractor network model of grid cell firing. J Neurosci 34: 5065–5079.

Buzsáki G. 2005. Theta rhythm of navigation: Link between path integration and landmark navigation, episodic and semantic memory. Hippocampus 15:827–840.

Cho J, Sharp PE. 2001. Head direction, place, and movement correlates for cells in the rat retrosplenial cortex. Behav Neurosci 115: 3–25.

Ekström, A.D, Kahana MJ, Caplan JB, Fields TA, Isham EA, Newman EL, Fried I. 2003. Cellular networks underlying human spatial navigation. Nature 425:184–188.

Ekström AD, Caplan JB, Ho E, Shattuck K, Fried I, Kahana MJ. 2005. Human hippocampal theta activity during virtual navigation. Hippocampus 15:881–889.

Fyhn M, Molden S, Witter MP, Moser EI, Moser MB. 2004. Spatial representation in the entorhinal cortex. Science 2004;305:1258–1264

Georges-François P, Rolls ET, Robertson RG. 1999. Spatial view cells in the primate hippocampus: Allocentric view not head direction or eye position or place. Cereb Cortex 9:197–212.

Green JD, Arduini A. 1954. Hippocampal activity in arousal. J Neurophysiol 17:533–557.

Green JD, Arduini AA. 1964. The hippocampus. Physiol Rev 44: 561–608.

Grossberg S, Pilly PK. 2012. How entorhinal grid cells may learn multiple spatial scales from a dorsoventral gradient of cell response rates in a self-organized map. PLoS Comput Biol 8:e1002648- doi: 10.1371/journal.pcbi.1002648

Guanella A, Kiper D, Verschure P. 2007. A model of grid cells based on a twisted torus topology. Int J Neural Syst 17:231–240.

Hafting T, Fyhn M, Molden S, Moser MB, Moser EI. 2005. Microstructure of a spatial map in the entorhinal cortex. Nature 436: 801–806.

Hasselmo ME. 2005. What is the function of hippocampal theta rhythm?—linking behavioral data to phasic properties of field potential and unit recording data. Hippocampus 15:936–949.

Hasselmo ME, Giocomo LM, Zilli EA. 2007. Grid cell firing may arise from interference of theta frequency membrane potential oscillations in single neurons. Hippocampus 17:1252–1271.

Hayman RM, Chakraborty S, Anderson MI, Jeffery KJ. 2003. Context-specific acquisition of location discrimination by hippocampal place cells. Eur J Neurosci 18:2825–2834.

Hayman R, Verriotis MA, Jovalekic A, Fenton AA. 2011. Anisotropic encoding of three-dimensional space by place cells and grid cells. Nat Neurosci 14:1182–1190. doi:10.1038/nn.2892

Heys JG, MacLeod K, Moss CF, Hasselmo M. 2013. Bat and rat neurons differ in theta frequency resonance despite similar spatial coding. Science 340:363–367.

Jeffery KJ, editor. 2003. The Neurobiology of Spatial Behaviour. Oxford University press. ISBN-10: 0198515243.

Jutras MJ, Fries P, Buffalo EA. 2013. Oscillatory activity in the monkey hippocampus during visual exploration and memory formation. Proc Natl Acad Sci 110:13144–13149. doi: 10.1073/pnas.1302351110

Kothari N, Wohlgemuth M, Hulgard K, Surlykke A, Moss CF. Timing matters: Sonar call groups facilitate spatio-temporal target

localization in bats. Front Physiol (2014) 5:168. doi: 10.3389/fphys.2014.00168.
Krupic J, Burgess N, O'Keefe J. 2012. Neural representations of location composed of spatially periodic bands. Science 337:853–857. doi: 10.1126/science.1222403.
Ledberg A, Robbe D. 2011. Locomotion-related oscillatory body movements at 6–12 Hz modulate the hippocampal theta rhythm. PLoS ONE. 6(11) e27575. DOI: 10.1371/journal.pone.0027575
Louie K, Wilson MA. 2001. Temporally structured replay of awake hippocampal ensemble activity during rapid eye movement sleep. Neuron 29:145–156.
Ludvig N, Tang HM, Gohil BC, Botero JM. 2004. Detecting location-specific neuronal firing rate increases in the hippocampus of freely-moving monkeys. Brain Res 1014:97–109.
Massoud TM, Horiuchi TK. 2011. A neuromorphic VLSI head direction cell system. IEEE Trans Circuits Syst I 58:150–163.
Mathis A, Stemmler M, Herz A. 2013. Optimal coding for 3D space: Grid cells of bats should spike on a face centered cubic lattice. Bernstein Conference, Tuebingen, Germany. doi: 10.12751/nncn.bc2013.0108
Matsumura N, Nishijo H, Tamura R, Eifuku S, Endo S, Ono T. 1999. Spatial- and task-dependent neuronal responses during real and virtual translocation in the monkey hippocampal formation. J Neurosci 19:2381–2393.
McGuire LP, Guglielmo CG, Mackenzie SA, Taylor PD. 2012. Migratory stopover in the long-distance migrant silver-haired bat, lasionycteris noctivagans. J Anim Ecol 81:377–385.
McNaughton BL, Battaglia FP, Jensen O, Moser EI, Moser MB. 2006. Path integration and the neural basis of the "cognitive map." Nat Rev Neurosci 7:663–678.
Mhatre H, Gorchetchnikov A, Grossberg S. 2012. Grid cell hexagonal patterns formed by fast self-organized learning within entorhinal cortex. Hippocampus 22:320–334. doi: 10.1002/hipo.20901.
Mizumori SJY. 2008. Hippocampal Place Fields. Oxford University Press. ISBN13: 9780195323245, ISBN10: 0195323246.
Moser EI, Kropff E, Moser MB. 2008. Place cells, grid cells, and the brain's spatial representation system. Annu Rev Neurosci 31:69–89.
Moss CF, Schnitzler H-U. 1995. Behavioral studies of auditory information processing. In: Fay RR, Popper AN, editors. Hearing by Bats. New York: Springer Verlag. pp 87–143.
Moss CF, Surlykke A. Probing the natural scene by echolocation. Front Behav Neurosci (2010) 4:33. doi: 10.3389/fnbeh.2010.00033
Moss CF, Bohn K, Gilkenson H, Surlykke A. 2006 Active listening for spatial orientation in a complex auditory scene. Pub Lib Sci Biol 4:615–626.
Muller R. 1996. A quarter of a century of place cells. Neuron 17:813–822.
Nishijo H, Ono T, Eifuku S, Tamura R. 1997. The relationship between monkey hippocampus place-related neural activity and action in space. Neurosci Lett 226:57–60.
O'Keefe J. 1976. Place units in the hippocampus of the freely moving rat. Exp Neurol 51:78–109.
O'Keefe J, Recce ML. 1993. Phase relationship between hippocampal place units and the EEG theta rhythm. Hippocampus 3:317–330.
Ono T, Nakamura K, Nishijo H, Eifuku S. 1993. Monkey hippocampal neurons related to spatial and nonspatial functions. J Neurophysiol 70:1516–1529.
Redish AD. 1999. Beyond the Cognitive Map. From Place Cells to Episodic Memory. MIT Press: Cambridge.
Robertson RG, Rolls ET, Georges-François P. 1998. Spatial view cells in the primate hippocampus: Effects of removal of view details. J Neurophysiol 79:1145–1156.
Rolls ET. 2002. Hippocampal spatial representations and navigation in primates. In: Sharp PE, editor. The Neural Basis of Navigation: Evidence from Single Cell Recording. Kluwer, Boston, MA. ISBN 978-1-4615-0887-8.
Rubin A, Yartsev MM, Ulanovsky N. 2014. Encoding of head direction by hippocampal place cells in bats. J Neurosci 34:1067–1080.
Sargolini F, Fyhn M, Hafting T, McNaughton BL, Witter MP, Moser MB, Moser EI. 2006. Conjunctive representation of position, direction, and velocity in entorhinal cortex. Science 312:758–762.
Siegel JJ, Neunuebel JP, Knierim JJ. 2008. Dominance of the proximal coordinate frame in determining the locations of hippocampal place cell activity during navigation. J Neurophysiol. 99:60–76.
Simmons JA, Ferragamo M, Moss CF, Stevenson S, Altes RA. 1990. Discrimination of jittered sonar echoes by the echolocating bat, eptesicus fuscus: The shape of target images in echolocation. J Comp Physiol A 167:589–616.
Stackman RW, Taube JS. 1998. Firing properties of rat lateral mammillary single units: Head direction, head pitch, and angular head velocity. J Neurosci 18:9020–9037. Erratum in: J Neurosci. 2003. 23:1555-1556.
Stensola H, Stensola T, Solstad T, Froland K, Moser M-B, Moser EI. 2012. The entorhinal grid map is discretized. Nature 492:72–76. doi:10.1038/nature11649
Surlykke A, Moss CF. 2000. Echolocation behavior of the big brown bat, eptesicus fuscus, in the field and the laboratory. J Acoust Soc Am 108:2419–2429. *[PMC]*[11108382*]*
Taube JS, Muller RU. 1998. Comparison of head direction cell activity in the postsubiculum and anterior thalamus of freely moving rats. Hippocampus 8:87–108.
Taube JS, Muller RU, Ranck JB Jr. 1990a. Head direction cells recorded from the postsubiculum in freely moving rats. I. Description and quantitative analysis. J Neurosci 10:420–435.
Taube JS, Muller RU, Ranck JB Jr. 1990b. Head direction cells recorded from the postsubiculum in freely moving rats. II. Effects of environmental manipulations. J Neurosci 10:436–447.
Tsoar A, Nathan R, Bartan Y, Vyssotski A, Dell'Omo G, Ulanovsky N. 2011. Large-scale navigational map in a mammal. Proc Natl Acad Sci 108:E718–724.
Ulanovsky N, Moss CF. 2007. Hippocampal cellular and network activity in freely-moving echolocating bats. Nat Neurosci 10:224–233.
Ulanovsky N, Moss CF. 2008. What the bat's voice tells the bat's brain. Proc Natl Acad Sci invited perspective. 105:8491–8498.
Ulanovsky N, Moss CF. 2011. Dynamics of hippocampal spatial representation in echolocating bats. Hippocampus 21:150–161.
Wiener SI, Taube JS. 2005. Head Direction Cells and the Neural Mechanisms of Spatial Orientation. Cambridge, MA: MIT Press.
Wilson MA, McNaughton BL. 1993. Dynamics of the hippocampal ensemble code for space. Science 261:1055–1058.
Yartsev M, Ulanovsky N. 2013. Representation of three-dimensional space in the hippocampus of flying bats. Science 340:367–372.
Yartsev MM, Witter MP, Ulanovsky N. 2011. Grid cells without theta oscillations in the entorhinal cortex of bats. Nature 479:103–107.
Zhang K. 1996. Representation of spatial orientation by the intrinsic dynamics of the head-direction cell ensemble: A theory. J Neurosci 16:2112–2126.